Title

Synthesis of cellulose nanofibril bound silver nanoprism for surface enhanced Raman scattering.

Journal

Biomacromolecules, 15(10)

ISSN

1525-7797

Authors

Jiang, Feng
Jiang, Feng
Hsieh, You-Lo

Publication Date

2014-10-01

DOI

10.1021/bm5011799

Peer reviewed

Article

pubs.acs.org/Biomac

Synthesis of Cellulose Nanofibril Bound Silver Nanoprism for Surface Enhanced Raman Scattering

Feng Jiang and You-Lo Hsieh*

Fiber and Polymer Science, University of California, Davis, California 95616, United States

Supporting Information

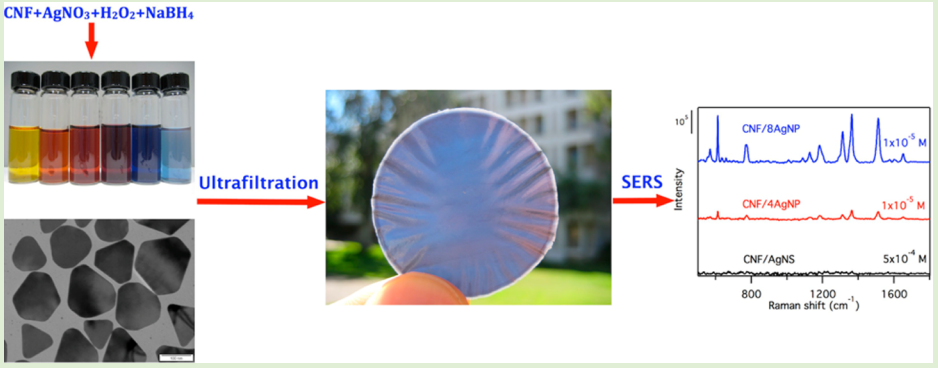

ABSTRACT: Silver nanoprisms (AgNPs) were robustly synthesized using TEMPO-oxidized cellulose nanofibrils (CNFs) as a dual capping and shape-regulating agent for the first time. Reducing $AgNO_3$ with $NaBH_4$ in CNF suspensions produced smaller but more uniform Ag nanospheres (AgNSs) with increasing Ag^+/CNF ratios. CNF bound AgNSs were facilely transformed to AgNPs by etching with H_2O_2, supporting the capping and shape-regulating capability of CNFs. AgNPs could also be synthesized directly in a one-shot reduction reaction with $NaBH_4$ in the presence of both CNFs and H_2O_2. The AgNPs transformed from CNF bound AgNSs are similar to those synthesized directly, but more stable against H_2O_2. Successful synthesis of AgNPs with 80−320 nm truncated edges was confirmed by light blue solution color, sharp out-of-plane quadruple resonance peak at 334 nm and prominent in-plane dipole resonance peaks at 762−900 nm. The [111] lattice plane of AgNP was clearly evident by its predominant XRD peak at 38°, confirming the unique shape-regulating ability of the nearly fully surface carboxylated CNFs. The CNF surface bound AgNPs were easily fabricated into freestanding CNF/AgNPs films that showed excellent surface enhanced Raman scattering of Rhodamine 6G with analytical enhancement factor of 5×10^3 in contrast to none from the CNF/AgNSs film.

INTRODUCTION

Silver nanoparticles are unique in their fascinating response to light via collective oscillation of free conduction band electrons coupled with an electromagnetic field of the incident light, giving localized surface plasmon resonance (LSPR).[1,2] LSPR induces strong light absorption and resonant scattering, as well as near-field enhancement of local electromagnetic fields by several orders of magnitude,[2−5] and is primarily controlled by the size and shape of silver nanoparticles.[6−8] This unusual size and shape-dependent property of silver nanoparticles has drawn special interest as they govern vast applications in catalysis,[9,10] sterilization,[11] optoelectronics,[12,13] surface enhanced Raman scattering (SERS),[14,15] metal-enhanced fluorescence,[16] biological imaging,[17] and sensors.[18−20]

Silver nanoprisms (AgNPs) are triangular-shaped single crystals with 40 nm to 1 μm long edges, 5−50 nm thickness, and face-centered cubic lattice structures, consisting of [111] crystal facets as the flat surfaces and [110] or [100] facets as the edges.[6] With increased edge length to thickness anisotropy, AgNPs have shown much superior plasmonic properties, such as more surface plasmon resonance peaks, much higher local electric field enhancement,[4] and stronger surface enhanced Raman scattering intensity.[21] The LSPR of AgNPs in the visible to near-infrared region has been achieved by adjusting their edge lengths, thickness, aspect ratios, and tip shapes[22−26] via either photochemical[8,24,26−31] or chemical[25,32−44] reduction. Among chemical reduction protocols, H_2O_2 aided AgNP synthesis has received most attention due to short reaction time (usually minutes), low energy consumption (without photoirradiation or thermal energy) and ease in size and shape control.[25] In the presence of trisodium citrate, H_2O_2 aided reduction has shown to be effective in converting variously shaped Ag nanowire,[39] nanocubes,[41] and bipyramids[41] into AgNPs. In fact, AgNPs could not be formed by replacing trisodium citrate with other carboxylate-containing molecules under photochemical reduction,[31] except for some diacids and

Received: June 12, 2014
Revised: September 2, 2014
Published: September 5, 2014

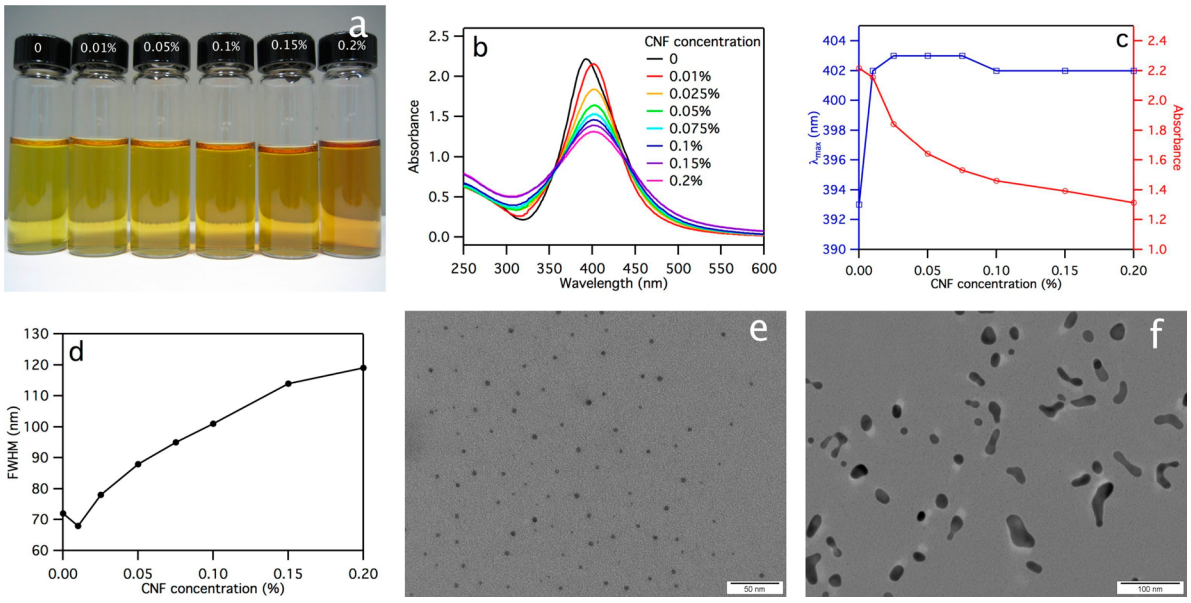

Figure 1. AgNS synthesis in the presence of CNFs at up to 0.2% concentrations: (a) aqueous suspensions, with CNF concentrations labeled; (b) UV−vis spectra; (c) λ_{max} and maximum absorbance; (d) fwhm; and TEM of AgNSs synthesized with (e) 0.01 and (f) 0.2% CNFs.

triacids with the nearest carboxylate groups separated by two carbons under H_2O_2 aided reduction.[39] It is widely accepted that trisodium citrate binds to the [111] facets of Ag nanoparticles to inhibit the growth along that axis, while permitting growth on the [100] facets[36,45] and such binding passivates Ag nanoparticle by reducing free energy, stabilizing against H_2O_2 etching, while allowing unpassivated Ag nanoparticles to be oxidized.[39,42]

Both sulfuric acid hydrolyzed cellulose nanocrystals (CNCs) and 2,2,6,6-tetramethylpyperidine-1-oxyl (TEMPO) oxidized cellulose nanofibrils (CNFs) have shown to serve as capping agents in the synthesis of spherical Ag nanoparticles.[46−53] As over 93% of CNF surface primary C6 hydroxyls could be converted to carboxylates by TEMPO oxidation,[54,55] the extensively surface carboxylated CNFs are hypothesized to serve as dual capping and shape-regulating agent in the synthesis of AgNPs. This study was therefore designed to investigate these dual roles of TEMPO oxidized CNFs. The ease to form CNF nanopaper by simple vacuum filtration[56,57] also enable direct fabrication of flexible cellulose nanofibrils/AgNPs to be tested for surface enhanced Raman scattering.

EXPERIMENTAL SECTION

Materials. Pure cellulose was isolated from rice straw (Calrose variety) by extraction with 2:1 v/v toluene/ethanol and subsequent dissolution of lignin and hemicellulose/silica with acidified $NaClO_2$ (1.4%, 70 °C, 5 h) and alkaline (5% KOH, 90 °C for 2 h), respectively.[58] Cellulose nanofibrils (CNFs) were defibrillated via TEMPO-mediated oxidation with 10 mmol NaClO per g of cellulose, followed by homogenization with mechanical blending at 37000 rpm for 30 min.[54] Silver nitrate ($AgNO_3$, Ultrapure grade, 99.5%, Acros Organics), sodium borohydride ($NaBH_4$, 98−99%, MP Biomedicals), hydrogen peroxide (H_2O_2, Certified ACS, 30%, Fisher Scientific), and Rhodamine 6G (dye content ∼ 95%, Sigma) were used as received without further purification. All water used was purified by a Milli-Q plus water purification system (Millipore Corporate, Billerica, MA)

Synthesis of Silver Nanospheres (AgNSs) and Nanoprisms (AgNPs). AgNSs were synthesized by reducing silver nitrate ($AgNO_3$) with excess sodium borohydride ($NaBH_4$) in the presence of varying amounts of CNFs (0−0.2 wt %) as capping agent. Typically, 40 μL of 50 mM $AgNO_3$ was added to CNF suspension and stirred for 1 min, then 200 μL of 100 mM ice-cooled $NaBH_4$ was added to make the total volume of 10 mL, and the solution was reacted for 40 min. Both $AgNO_3$ and $NaBH_4$ solutions were freshly prepared during the day of the reaction, and $NaBH_4$ was placed in ice to minimize decomposition.

AgNPs were synthesized following two reaction routes: AgNSs transformation and direct conversion. In transforming AgNSs to AgNPs, varying quantities of H_2O_2 (0−80 μL) were added to AgNSs synthesized as above (40 min after $NaBH_4$ addition). The as-synthesized suspension was centrifuged (14000 rpm, 30 min) to precipitate AgNPs, and the supernatant was digested using nitric acid, and the total silver content was quantified using inductively coupled plasma atomic emission spectroscopy (ICP-AES, Thermo iCAP6500) at a wavelength of 328.068 nm to determine the conversion efficiency. In a direct conversion reaction, 40 μL of 50 mM $AgNO_3$ was added to a CNF suspension (0.1 and 0.2 wt %), stirred for 1 min, then H_2O_2 (10−240 μL for 0.1 wt % CNFs, and 20−80 μL for 0.2 wt % CNFs) was added and stirred for another 1 min, and finally, 200 μL of 100 mM ice-cooled $NaBH_4$ was added to make the total volume of 10 mL, and the solution was allowed to react for 40 min.

Characterization of AgNSs and AgNPs. Extinction spectra of the solutions were measured in the 250−900 nm range using Evolution 600 UV−vis spectrophotometer (Thermo Scientific). For imaging AgNSs, the as-synthesized suspension was diluted 50 times, and 10 μL of the dilute suspension was deposited onto glow-discharged, carbon-coated TEM grids (300-mesh copper, Formvar-carbon, Ted Pella Inc., Redding, CA) and dried under ambient condition. For imaging AgNPs, the as-synthesized suspension was centrifuged at 14000 rpm for 30 min in order to remove any unbound CNFs. The precipitate was collected, redispersed, then diluted 50 times, and deposited onto glow-discharged, carbon-coated TEM grids. The samples were observed using a Philip CM12 transmission electron microscope operated at a 100 kV accelerating voltage.

Fabrication of CNF/Ag Nanocomposite Film. To fabricate CNF/Ag nanocomposite film, 50 mL of 0.2 wt % CNF suspension containing varying amounts of AgNSs or AgNPs was filtered (nylon membrane, 200 nm pore size, Millipore, Billerica, MA) for around 8 h to CNF hydrogel that was detached, pressed between two nylon membranes, and dried at 80 °C. Pure CNF suspension was used to fabricate CNF film as control. AgNSs were synthesized by reducing $AgNO_3$ with 0.01 wt % CNFs as before to which more concentrated CNF suspension was added to raise CNF concentration to 0.2 wt % while keeping AgNSs at 8 μmol. AgNPs were synthesized by transforming AgNSs synthesized with 0.2 wt % CNFs by adding 60

dx.doi.org/10.1021/bm5011799 | Biomacromolecules 2014, 15, 3608−3616

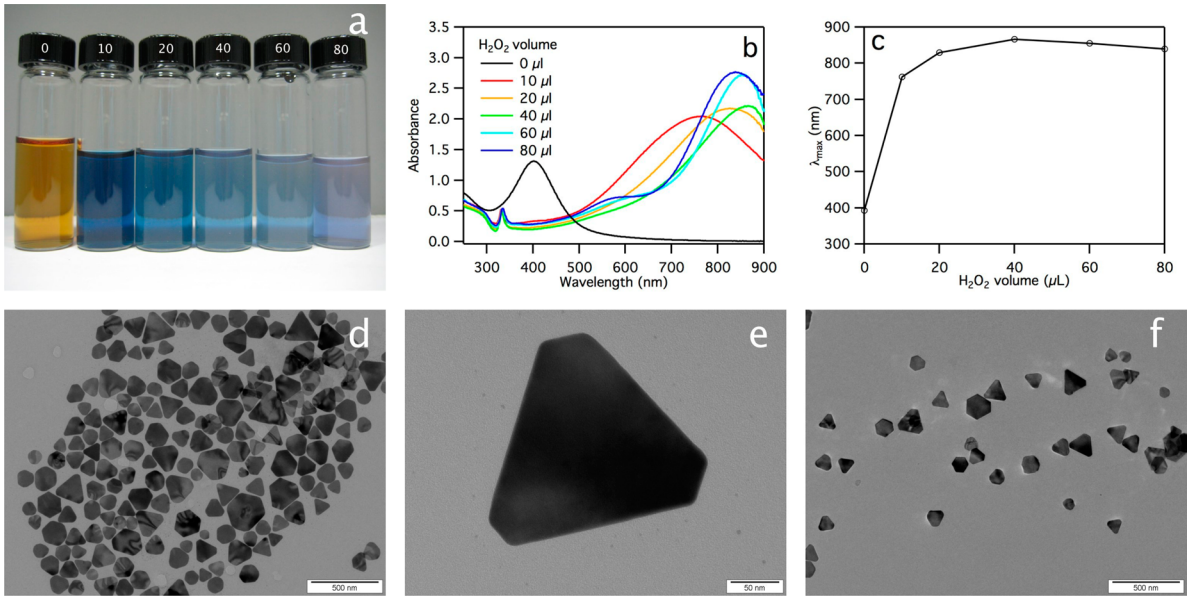

Figure 2. AgNPs transformed with the post-addition of H_2O_2 (0−80 μL) in the presence of 0.2% CNFs: (a) aqueous suspensions with H_2O_2 quantities in μL labeled; (b) UV−vis spectra; (c) λ_{max} vs H_2O_2 volume; TEM images of AgNPs formed with post-addition of (d, e) 60 and (f) 80 μL of H_2O_2.

μL of H_2O_2, as described in a previous section, and the AgNP amounts were kept at 4 and 8 μmol with the addition of extra 0.2 wt % CNFs to a total of 50 mL of suspension. The CNF/Ag nanocomposite films containing 8 μmol AgNSs, 4 and 8 μmol AgNPs were designated as CNF/AgNS, CNF/4AgNP, and CNF/8AgNP, respectively.

Characterization of CNF/Ag Nanocomposite Film. The light transmittance of a CNF/Ag nanocomposite film was measured in the 250−900 nm region using an Evolution 600 UV−vis spectrophotometer. The elemental compositions of the CNF/Ag naocomposite film were measured using the EDS (X-Max^N Silicon Drift Detector, Oxford Instruments, Abingdon, Oxfordshire, England) adjunct to the SEM at a magnification of 500× with a 12 kV accelerating voltage and a 5 mm working distance. XRD spectra for CNF/Ag nanocomposite films were collected on a Scintag XDS 2000 powder diffractometer using a Ni-filtered Cu Kα radiation (λ = 1.5406 Å) at an anode voltage of 45 kV and a current of 40 mA from 5° to 90° at a scan rate of 2°/min.

Surface Enhanced Raman Spectroscopy. CNF/Ag nanocomposite film (5 mm × 5 mm) was immersed in aqueous fluorescent dye Rhodamine 6G (10 mL, 1 μM to 5 mM) for 1 h, then rinsed with water and dried under ambient conditions. Raman scattering spectra of Rhodamine 6G adsorbed CNF/Ag nanocomposite films were obtained using a Renishaw RM1000 spectrometer at 785 nm excitation with 20s acquisition time and an objective magnification of 50×.

RESULTS AND DISCUSSION

Characteristics of CNFs. Combined TEMPO-mediated oxidation (10 mmol NaClO/g of cellulose) and mechanical blending (37000 rpm, 30 min) has shown to facilely isolate CNFs with about 2 nm widths and a few hundreds to thousand nm lengths (Supporting Information, Figure S1).[54] The surface carboxylate contents were determined to be 1.68 mmol/g of cellulose or over 93% conversion of surface primary hydroxyls.[55] Assuming a cylindrical cross-section with a 2 nm diameter and 1.6 g/cm^3 bulk density, the surface carboxylate density on CNFs is calculated to be −0.81 e/nm^2. All CNF carboxylates are preserved in sodium salt form under basic pH 10 after TEMPO oxidation to facilitate binding with Ag^+ while avoiding an increased acidity of carboxylic for AgNPs synthesis.

Effects of CNF Concentrations on AgNSs. Reducing silver precursor $AgNO_3$ with $NaBH_4$ at 10:1 $NaBH_4/AgNO_3$ molar ratio without CNFs turned the aqueous solution immediately to golden yellow, indicative of AgNSs that were also confirmed by the 393 nm UV−vis absorption peak (Figure 1a, b), characteristic surface plasmon resonance of AgNSs. The clear golden yellow solution indicated well-dispersed AgNSs, possibly due to the stabilizing effect of excess borohydride ions. In the presence of CNFs, the same reduction reaction produced a pale yellow solution immediately, which then turned golden yellow after approximately 20 min with the final colors darkening with increasing CNF concentrations. UV−vis spectra of all solutions from reduction with CNFs showed λ_{max} at 402 nm, slightly higher than that at 393 nm without CNFs. Surface plasmon resonance peak shifting of Ag nanoparticles has been ascribed to many factors including refractive index of the surrounding medium,[59] capping ligands,[60,61] surface oxidation,[62] and particle size.[63] The λ_{max} red-shifted from 393 to 402 nm observed with CNFs is thought be due to the adsorption of carboxylated CNFs on the AgNS surfaces. A similar red-shift from 390 to 413 nm has been observed by adsorption of oleate on the silver nanoparticles.[61] The initial pale yellow color is consistent with Ag^+ binding to the CNF surface carboxylates and hydroxyls by electrostatic and ion-dipole interactions, respectively, followed by a reduction to zero valence Ag atom by $NaBH_4$, then coalesce into AgNSs, exhibiting golden yellow color. The gradual darkening in colors showed the subsequent growth of CNF bound Ag clusters into larger AgNSs to be slow. As the CNF concentrations increased from 0.01 to 0.2%, the λ_{max} remained at 402 nm, but the maximum absorbance decreased, and the full width at half-maximum (fwhm) increased (Figure 1c,d), again reflecting the increased AgNS sizes and heterogeneity that were further confirmed by TEM (Figure 1e,f). AgNSs synthesized with 0.01% CNF were small (3.5 ± 1.1 nm) and relatively homogeneous (Figure 1e), whereas those produced at 0.2% CNF were much larger and more elongated (Figure 1f), consistent with the darker yellowish color.

dx.doi.org/10.1021/bm5011799 | Biomacromolecules 2014, 15, 3608−3616

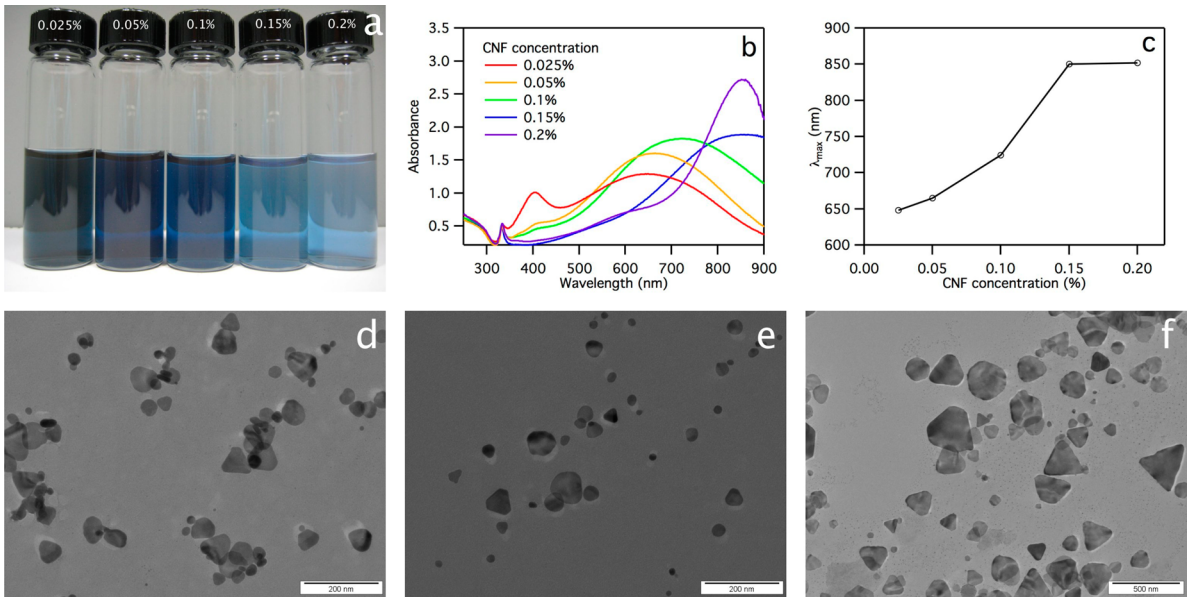

Figure 3. AgNPs transformed with post addition of 60 μL H_2O_2 in the presence CNFs at up to 0.2% concentrations: (a) aqueous suspensions, with CNF concentration labeled; (b) UV–vis spectra; (c) λ_{max} vs CNF concentration; TEM images of AgNPs formed with (d) 0.05, (e) 0.1, and (f) 0.15% CNFs.

With increasing CNF concentrations from 0.01 to 0.2%, the COO^-/Ag^+ ratio increases from 0.84 to 16.8, showing excess COO^- in all cases except for 0.01% CNF. With added $AgNO_3$, Ag^+ could bind with COO^- by replacing Na^+, as previously confirmed.[64] At lower CNF concentrations, both bound and free Ag^+ could be rapidly reduced by $NaBH_4$, while free Ag atoms could nucleate with other free and bound Ag and grow quickly into small uniform AgNSs (Supporting Information, Scheme S1). At higher CNF concentrations with COO^- in excess, most Ag^+ would bind with the CNF surface COO^- and reduce to zero valence Ag atoms while still being attached to the CNF surfaces. Nucleation and growth of the bound Ag atoms would occur slowly upon release and migration of some bound Ag atoms to grow on the existing nuclei, leading to more heterogeneous sizes. Selective binding of CNF surface carboxylates to specific facets of AgNSs, such as the [111] facets, would allow growth along the other facets into more elongated shapes. The more elongated AgNSs gave the first indication of potential spatial effects of CNF as a capping agent.

Anisotropic AgNPs from etching of AgNSs. AgNSs synthesized with 0.2% CNFs were transformed into AgNPs via H_2O_2 etching. Upon adding H_2O_2 (10–80 μL), the solution color turned immediately from yellow to blue, then lightened with increasing H_2O_2 quantities (Figure 2a) along with the observation of bubbles, likely from decomposition of H_2O_2 (Supporting Information, Video S1). The UV–vis absorption spectra of all H_2O_2-containing solutions showed AgNP characteristic peaks, that is, out-of-plane quadrupole resonance at 334 nm, as well as increasing in-plane dipole resonance from 762 to 866 nm, but none at 402 nm (Figure 2b,c). The complete absence of the surface plasmon resonance peak for AgNSs (402 nm) and the presence of the AgNP characteristic peaks (334 nm, 762 to 866 nm) give clear evidence of immediate and increasing transformation of AgNSs to AgNPs with the addition of H_2O_2. Although the solution turned blue with the addition of 20 μL of H_2O_2 and showed in-plane dipole resonance at 829 nm, the broad peak (Figure 2b) and irregularly shaped nanoparticles (Supporting Information, Figure S2) indicated 20 μL of H_2O_2 to be insufficient to convert all AgNSs to AgNPs. With 60 and 80 μL of H_2O_2, all AgNSs were transformed to AgNPs, showing 80–200 nm long truncated edges (Figure 2d–f). The conversion efficiency of Ag^+ to AgNPs was further determined using ICP-AES. For AgNPs synthesized with 40, 60, and 80 μL of H_2O_2, approximately 96.2, 97.8, and 98.0% of Ag^+ were converted to AgNPs, respectively. Such high conversions are close to the nearly 100% yield of AgNPs synthesized using trisodium citrate,[39,42] indicating CNFs to be highly efficient in forming AgNPs.

AgNSs to AgNPs transformation was further investigated at a constant and optimal 60 μL H_2O_2 but varied CNF concentrations (0.025 to 0.2%; Figure 3). Upon adding H_2O_2 to AgNSs synthesized with 0.025% CNF, the solution changed from yellowish (Figure 1a) immediately to dark blue (Figure 3a) while exhibiting two UV–vis peaks at 400 and 650 nm, corresponding to AgNS surface plasmon resonance and AgNP in-plane dipole surface plasmon resonance peaks, respectively (Figure 3b), and showing the coexistence of AgNSs and AgNPs. The blue color became less intense (Figure 3a), while the AgNS peak at 400 nm decreased in intensity with increasing CNF concentrations and completely disappeared at 0.15% CNFs and above (Figure 3b). All solutions showed the small sharp out-of-plane quadrupole surface plasmon resonance peak of AgNPs at 334 nm while the in-plane dipole surface plasmon resonance peak increased in λ_{max} from 650 to 850 nm at 0.15% CNFs and above (Figure 3c). The narrower and higher intensity of the 850 nm AgNP peak observed at 0.2% CNF suggested more uniform size and shape than those at 0.15% CNF (Figure 3b). The shapes and sizes of AgNPs formed at lower CNF concentrations were highly irregular (Figure 3d–f). Both improved with increasing CNF concentration to 0.15% and 0.2% (Figure 2d).

The cellulose Iβ crystalline unit cell structure show the spacings between adjacent surface C6s are 1.038 nm along the *c* axis (chain direction), 0.663 nm between adjacent 002 planes, and 0.778 nm between three 002 plane (Scheme 1a,b). With

dx.doi.org/10.1021/bm5011799 | *Biomacromolecules* 2014, 15, 3608–3616

Scheme 1[a]

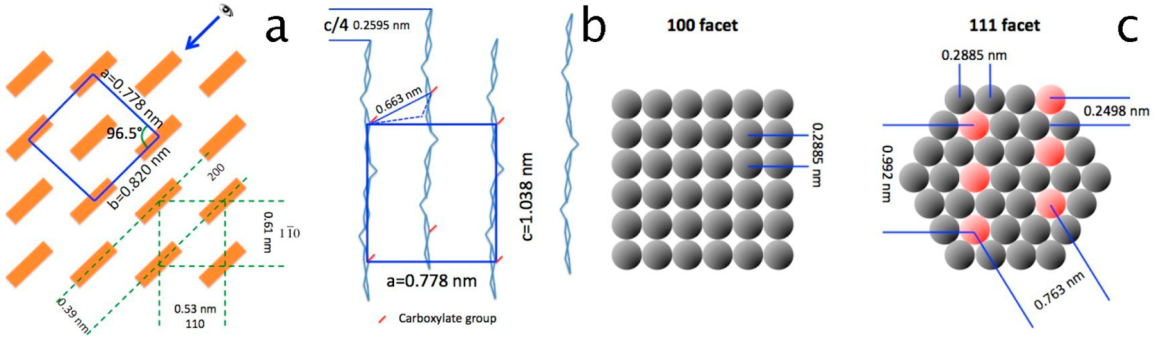

[a](a) Cellulose Iβ crystal containing 16 chains; (b) side view of a in the arrow direction (Adapted from Imai et al. Geometric phase analysis of lattice images from algal cellulose microfibrils. *Polymer* **2003**, *44*, 1871−1879. Copyright 2003, with permission from Elsevier.[65]). Solid lines represent unit cell with dimensions of a = 0.778 nm, b = 0.820 nm, c = 1.038 nm, and γ = 96.5°;[66] dash lines represent 110, 1$\bar{1}$0, and 200 lattice planes with respective d-spacings of 0.53, 0.61, and 0.39 nm; (c) 100 and 111 facets of the fcc unit cell of Ag.

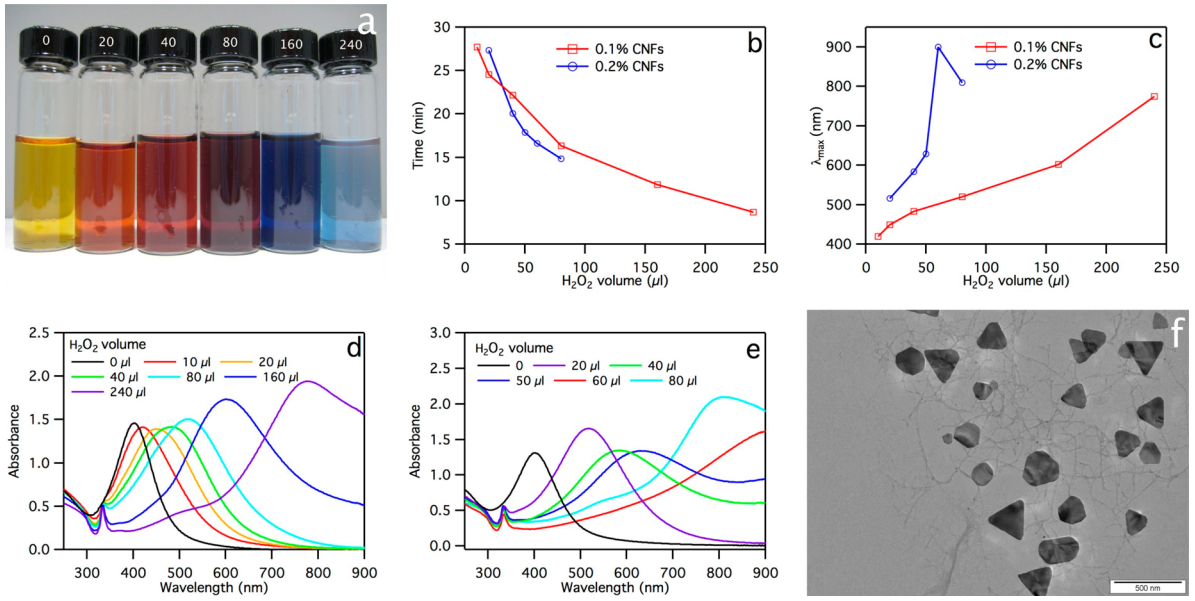

Figure 4. AgNPs synthesis in the presence of 0.1 and 0.2% CNFs with 0−240 μL H_2O_2 (indicated in a, d, and e): (a) colors of 0.1% CNF aqueous suspensions; (b) time lag between adding $NaBH_4$ and color change; (c) λ_{max}; UV−vis spectra with (d) 0.1 and (e) 0.2% CNFs; (f) TEM of AgNPs synthesized with 0.2% CNF and 60 μL H_2O_2.

93% of surface C6 primary hydroxyls converted, the CNF surface C6s are nearly fully carboxylated. Assuming all the adjacent C6 primary hydroxyls exposed on the surface were carboxylated, these spacings between CNF surface C6s are much greater than that between the dicarboxylic acid groups in sodium citrate (2.72−2.98 Å).[45] The [100] and [111] facets of fcc unit cell of Ag (Scheme 1c) shows that the spacings between Ag atoms (shown in red) in the hexagonal [111] facet are closer to the spacing between CNF carboxylates than those in the square [100] facet so the two adjacent CNF surface carboxylates may preferentially bind the Ag atoms in [111] facet via silver−oxygen bonds similarly to sodium citrate to inhibit the growth along that axis. In contrast to sodium citrate that binds Ag atoms by closely matching the spacing between adjacent carboxylates, bindings of CNFs on the [111] facet of Ag may not be as exactly matched spatially, but the inhibiting and covering effects were similar because of the multiple carboxylates along the very long and flexible CNFs. By selectively binding to the [111] facets of Ag nanoparticles, CNFs protect the [111] facets while allowing H_2O_2 etching on other facets to transform AgNSs into AgNPs. While Ag nanospheres have been transformed to nanoprisms with sodium citrate and other dicarboxylate and tricarboxylate compounds with the nearest carboxylate groups separated by two carbons,[39,41] nearly fully surface carboxylated cellulose nanofibrils have clearly shown to also facilitate this conversion. This is the first evidence of passivation by nonsoluble nanofibrillar solids on such transformation.

Synthesis of Anisotropic AgNPs. AgNPs were also synthesized by reducing $AgNO_3$ precursor in the presence of both capping CNF and etching H_2O_2 reagents, that is, 10−240 μL H_2O_2 in 0.1% CNF and 20−80 μL of H_2O_2 in 0.2% CNF suspensions. Upon adding $NaBH_4$, the colorless $AgNO_3$/CNFs/H_2O_2 mixtures turned pale yellow initially, indicating formation of Ag clusters, then changed to drastically different colors ranging from orange, brown, purple, blue, and cyan. The time taken to reach these final colors shortened with increasing H_2O_2 quantities. Substantial bubbles were also released, likely from the decomposition of H_2O_2 and $NaBH_4$ into O_2 and H_2 (Supporting Information, Video S2).

dx.doi.org/10.1021/bm5011799 | *Biomacromolecules* 2014, 15, 3608−3616

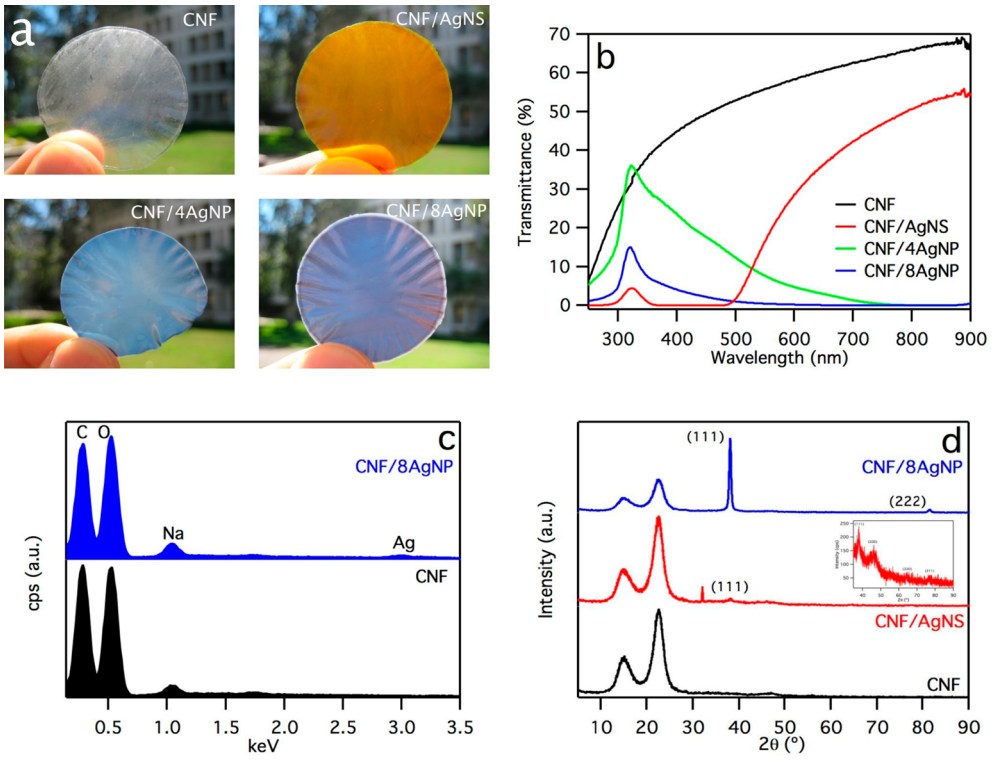

Figure 5. CNF and CNF/Ag nanocomposite films: (a) Photographs; (b) UV−vis transmittance spectra; (c) EDS spectra of CNF and CNF/8AgNP; (d) XRD spectra.

At 0.1% CNF, the final colors of yellow, orange, purple, blue, and cyan were observed in decreasing lengths of time from 28 to 9 min with increasing H_2O_2 from 10 to 240 μL (Figure 4a,b). These colors clearly indicated the formation of anisotropic Ag nanoplates. Similar color changes with increased H_2O_2 amount were also observed with 0.2% CNF, but in slightly shorter times. The successful synthesis of AgNPs was confirmed by the AgNP characteristic out-of-plane quadrupole resonance peak at 334 nm, which increased in sharpness with increasing amount of H_2O_2 (Figure 4c−e). With increasing H_2O_2 quantities, the nanoprism in-plane dipole resonance peaks shifted to higher wavelength ranges of 420−775 nm (Figure 4d) and 516−900 nm (Figure 4e) with 0.1 and 0.2% CNFs, respectively. In addition, small shoulders near 500 nm appeared with more H_2O_2, that is, 160 and 240 μL at 0.1% CNF, and 60 and 80 μL at 0.2% CNF, and were assigned to AgNP out-of-plane dipole resonance. The in-plane dipole resonance, characteristics of anisotropic Ag nanoplates, showed increased λ_{max} with increasing H_2O_2, from 420 to 775 nm with 0.1% CNF (10−240 μL H_2O_2) and more drastically from 516 to 900 nm with 0.2% CNF (20−60 μL H_2O_2; Figure 4c). In the latter case, the decrease in λ_{max} at 80 μL of H_2O_2 is due to reduced AgNP sizes from etching, again confirmed by TEM (Supporting Information, Figure S3). Besides, the λ_{max} of in-plane dipole resonance is always higher at 0.2% CNF than that at 0.1% CNFs, indicating less H_2O_2 is needed to synthesize AgNPs at higher CNF concentrations. The TEM images clearly showed triangular-shaped AgNPs with edge lengths ranging from 100 to 300 nm among a CNF network structure (Figure 4f), along with some smaller spherical nanoparticles (Supporting Information, Figure S4), indicating partial formation of AgNPs. As AgNPs were precipitated from centrifugation, unbound CNFs would remain in the suspension. The observation CNFs along with AgNPs supports the CNF bound nature of AgNPs.

The fact that AgNPs could be synthesized with 80 μL of H_2O_2 at 0.2% CNF concentration whereas substantially more H_2O_2 (240 μL) was necessary at 0.1% CNF concentration attest to the unique dual capping and shape-regulating role of CNFs. With more CNF present in the solution, Ag clusters are better protected from oxidization by H_2O_2 and stabilized by being bound to CNF to allow more effective etching with less H_2O_2, leading to significantly reduced reaction time and less H_2O_2 consumption.

In AgNP synthesis by either method, both H_2O_2 and CNFs are essential in forming more homogeneous AgNPs. In AgNP synthesis in the presence of both reducing agent $NaBH_4$ and etching agent H_2O_2, reduction and oxidization occur simultaneously. H_2O_2 oxidizes uncapped Ag nanoparticles into Ag cations which were then further reduced by $NaBH_4$ to atomic Ag then onto CNF passivated Ag nanoparticles to form AgNPs. As most of the AgNP surfaces were capped by CNFs, these capped surfaces were most stable against H_2O_2 etching. Therefore, the net effect of H_2O_2 is to oxidize uncapped less stable Ag nanoparticles and promote the growth of AgNPs.[39] Therefore, the amount of H_2O_2 is critical in controlling both kinetics and yields of AgNPs. CNFs passivate the [111] facets of Ag nanoparticles by their surface carboxylates, while permitting Ag nanoparticle growth only along the [100] facets into anisotropic AgNPs. With more CNFs, the [111] facets were more fully passivated to synthesize more homogeneous AgNPs. While AgNPs could be synthesized with 0.2% CNFs and 60 μL H_2O_2 via both methods, transformation from AgNSs shows full conversion and more uniform AgNP sizes and shapes as well as better stability against H_2O_2 etching. Besides, more spherical nanoparticles could be

dx.doi.org/10.1021/bm5011799 | Biomacromolecules 2014, 15, 3608−3616

observed in the one shot synthesized sample as compared to those transformed from AgNSs. Therefore, AgNPs synthesized by transformation of AgNSs were made into films for surface enhanced Raman scattering characterization.

Fabrication and Characterization of CNF/Ag Nanocomposite Films. CNF/Ag nanocomposite films were fabricated from 0.2% CNF series with varying AgNS or AgNP quantities. The control CNF film contained no Ag and appeared translucent (Figure 5a), transmitting 45 to 70% in the visible light range (Figure 5b). The opaqueness is likely due to CNF aggregation from vacuum filtration and drying. The CNF/AgNS film containing 8 μmol AgNSs appeared brown whereas those with 4 and 8 μmol of AgNPs, or CNF/4AgNP and CNF/8AgNP, respectively, were blue, all in similar colors as their respective solutions. CNF/AgNS film absorbed more visible light in the lower wavelength range due to the spherical nature of AgNSs, but transmitted increasing extents in the 500−900 nm wavelength range to 55% at 900 nm. Both CNF/4AgNP and CNF/8AgNP films transmitted some light in the lower wavelengths, that is, 300−720 and 300−520 nm, respectively, but absorbed all light above these regions, as expected of AgNPs (Figure 5b). The transmittance decreased with increased amount of AgNPs. These films are flexible, bending freely when squeezed between fingers without breaking (Supporting Information, Figure S5). Tensile strength and Young's modulus of TEMPO-oxidized cellulose films have been reported to be 200−300 MPa and 6−7 GPa.[67] The EDS spectra showed 1.2 At% Na atomic concentration for CNF film, reflecting the presence of sodium carboxylate on the CNF surfaces, and the Na content increased to 2.0, 2.5, and 2.4 At% for CNF/AgNS, CNF/4AgNP, and CNF/8AgNP, respectively, possibly due to the additional Na absorption from $NaBH_4$ (Figure 5c, Table 1). Although the original CNF/AgNS and CNF/8AgNP solutions had the same 8 μmol Ag concentration, 0.28, 0.2, and 0.38 At% Ag was detected on CNF/AgNS, CNF/4AgNP, and CNF/8AgNP, respectively. The lower atomic Ag concentration in CNF/AgNS film is likely due to losing the small and unattached AgNSs in vacuum filtration. The nearly doubled Ag content in CNF/8AgNP than that in CNF/4AgNP is consistent with the doubled initial concentration. The fact that Ag content in CNF/AgNP films is consistent to the initial Ag concentration further supports that the AgNPs are strongly bound to CNFs and fully retained in both films. For CNF/8AgNP, a sharp dominant peak at 38° in the XRD spectrum gave the clear evidence of the [111] lattice plane of face-centered cubic (fcc) silver (JCPCDS 4−783). The predominant [111] basal faces confirmed that the AgNPs are primarily bound to CNFs at the [111] plane (Figure 5d). A barely visible peak at 82° was assigned to the [222] lattice plane, one of the side faces. No other peaks could be observed in CNF/8AgNP, indicating lacking specific order of all the other facets thus not be detected by XRD. In contrast, XRD of CNF/AgNS showed peaks at 38, 44, 64, and 77°, corresponding to all [111], [200], [220], and [311] fcc crystal planes of the AgNSs, although at very low intensities. The appearance of all fcc crystal facets in CNF/AgNS confirms its isotropic nature while the low intensity reflects the low quantity of AgNSs. The XRD spectra of all films exhibited clear cellulose I crystalline structure between 10 and 30° same as reported for CNFs alone.[68,69]

Table 1. Atomic Compositions of CNF/Ag Nanocomposite Films Quantified by EDS

	atomic composition (%)			
samples	C	O	Na	Ag
CNFs	59.0 ± 0.2	39.8 ± 0.2	1.2 ± 0.1	N/A
CNF/AgNS	55.5 ± 0.2	42.3 ± 0.1	2.0 ± 0.1	0.28 ± 0.04
CNF/4AgNP	56.1 ± 1.1	41.2 ± 1.2	2.5 ± 0.1	0.2
CNF/8AgNP	55.4 ± 1.5	41.9 ± 1.6	2.4 ± 0.2	0.38 ± 0.05

Surface Enhanced Raman Scattering of CNF/Ag Nanocomposite Films. Fluorescent dye was adsorbed in CNF/Ag nanocomposite films by immersion in aqueous Rhodamine 6G solution for 1 h. The sensitivity of surface enhanced Raman scattering (SERS) of CNF/AgNS and CNF/AgNP was examined (Figure 6a). From adsorption of 10^{-5} M Rhodamine 6G, both CNF/4AgNP and CNF/8AgNP showed sharp Rhodamine 6G characteristic peaks, that is, 611, 773, and 1127 cm^{-1} peaks for C−C−C ring in-plane bending vibration, C−H out-of-plane bending vibration and C−H in-plane bending vibration, respectively, while showing aromatic stretching vibrations at 1310, 1360, 1507, and 1648 cm^{-1}.[70] The much stronger peak intensities for CNF/8AgNP over those for CNF/4AgNP showed the SERS sensitivity to be AgNPs concentration dependent. In contrast, Raman scattering peaks for Rhodamine 6G were not detected on CNF/AgNS, even with an order of magnitude higher 5×10^{-4} M Rhodamine 6G concentration. This is expected as spherical AgNSs do not absorb nor induce oscillation of the conduction electron at the 785 nm laser beam wavelength used for excitation, resulting in no enhancement of the local electric field and therefore do not show SERS properties (Figure 5b). In contrast, AgNPs interacted strongly with the light at 785 nm (Figure 5b), and the local electric field was greatly enhanced to form hot spots showing significant enhancement of Raman scattering.

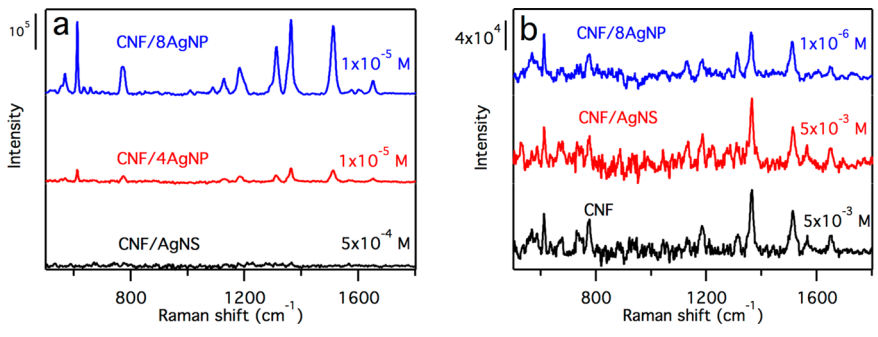

Figure 6. Surface enhanced Raman scattering of Rhodamine 6G with various concentrations obtained from the CNF/Ag nanocomposite films.

dx.doi.org/10.1021/bm5011799 | Biomacromolecules 2014, 15, 3608−3616

To quantify the SERS enhancement factor, Raman spectra of Rhodamine 6G on CNF, CNF/AgNS, and CNF/8AgNP were recorded and shown in Figure 6b. The analytical enhancement factor (AEF) was calculated from eq 1:[71]

$$\mathrm{AEF} = \frac{I_{\mathrm{SERS}}/c_{\mathrm{SERS}}}{I_{\mathrm{CNF}}/c_{\mathrm{CNF}}} \quad (1)$$

where I_{SERS} and I_{CNF} are the Raman signal intensities for CNF/Ag and CNF, respectively, and c_{SERS} and c_{CNF} represent the Rhodamine 6G concentrations in the detecting solution for CNF/Ag and CNF, respectively. The Raman scattering intensity of Rhodamine 6G on CNF/AgNS is similar to that on CNF film, both showing no absorption at 785 nm or lacking SERS as expected (Figure 6b). On the other hand, the CNF/8AgNP film showed a significant enhancement, with 5.7×10^3, 6.9×10^3, 3.7×10^3 and 4.4×10^3 calculated AEF values for the 611, 1310, 1360, and 1507 cm^{-1} Raman peaks, respectively. These over 3 orders of magnitude increases in Raman signal enhancement are highly impressive, showing excellent capability of detecting target molecules at the sub part-per-million (PPM) level. These data show that CNF/AgNPs are superior substrates for surface enhanced Raman scattering, capable of detection at significantly lowering limits.

CONCLUSIONS

Cellulose nanofibrils (CNFs) with 1.68 mmol/g surface carboxylates spaced approximately 0.67−1.04 nm apart have demonstrated to be highly effective as dual capping and shape-regulating agents in the synthesis of silver nanospheres (AgNSs) and nanoprisms (AgNPs). Uniformly small (3.5 nm) AgNSs could be synthesized at low CNF concentration as 0.01%, then grew in sizes and heterogeneity in shapes with increasing CNF concentrations. The CNF bound AgNSs were facilely transformed into AgNPs by adding etching agent H_2O_2, as evidenced by the disappearance of the AgNS characteristic peak at 402 nm and the appearance of a new out-of-plane quadrupole resonance (334 nm) and in-plane dipole resonance (762−866 nm) peaks, characteristic of AgNPs. Most uniform AgNPs with edge lengths ranging from 80 to 200 nm were produced in the presence of 0.2% CNF and 60 μL of H_2O_2. AgNPs were also synthesized by $NaBH_4$ reduction in the presence of H_2O_2, showing tunable in-plane dipole resonance peaks ranging from 420 to 900 nm, indicating the gradual evolution of AgNPs. CNF bound AgNPs could be robustly synthesized with 0.2% CNFs and 60 μL of H_2O_2 by both methods, with the post-transformed AgNPs being more stable in the presence of a higher H_2O_2 amount of 80 μL. Both CNF bound AgNSs and AgNPs could be facilely fabricated into flexible CNF/Ag nanocomposite films via vacuum ultrafiltration. CNF/AgNP film showed excellent enhancement on the Raman scattering with impressive analytical enhancement factor exceeding 3 orders of magnitude, whereas the CNF/AgNS film showed none.

ASSOCIATED CONTENT

Supporting Information

AFM height image and profile of CNF. Scheme for AgNSs synthesis at low and high CNF concentrations. TEM images of AgNPs formed with post addition of 20 μL of H_2O_2 at 0.2% CNF. TEM of AgNPs synthesized with 0.2% CNF and 60 and 80 μL H_2O_2. Images of CNF/Ag nanocomposite files squeezed with fingers. Video clips of the transformation of AgNSs to AgNPs (Video S1) and the one-shot synthesis of AgNPs (Video S2). This material is available free of charge via the Internet at http://pubs.acs.org.

AUTHOR INFORMATION

Corresponding Author

*E-mail: ylhsieh@ucdavis.edu. Fax: +1 530 752 7584. Tel.: +1 530 752 0843.

Notes

The authors declare no competing financial interest.

ACKNOWLEDGMENTS

Financial support for this research from the California Rice Research Board (Project RU-9) is greatly appreciated.

REFERENCES

(1) Wiley, B. J.; Im, S. H.; Li, Z. Y.; McLellan, J.; Siekkinen, A.; Xia, Y. N. *J. Phys. Chem. B* **2006**, *110*, 15666−15675.
(2) Hutter, E.; Fendler, J. H. *Adv. Mater.* **2004**, *16*, 1685−1706.
(3) Pastoriza-Santos, I.; Liz-Marzan, L. M. *J. Mater. Chem.* **2008**, *18*, 1724−1737.
(4) Hao, E.; Schatz, G. C. *J. Chem. Phys.* **2004**, *120*, 357−366.
(5) Jain, P. K.; Huang, X. H.; El-Sayed, I. H.; El-Sayed, M. A. *Acc. Chem. Res.* **2008**, *41*, 1578−1586.
(6) Millstone, J. E.; Hurst, S. J.; Metraux, G. S.; Cutler, J. I.; Mirkin, C. A. *Small* **2009**, *5*, 646−664.
(7) Xia, Y. N.; Xiong, Y. J.; Lim, B.; Skrabalak, S. E. *Angew. Chem., Int. Ed.* **2009**, *48*, 60−103.
(8) Bastys, V.; Pastoriza-Santos, I.; Rodriguez-Gonzalez, B.; Vaisnoras, R.; Liz-Marzan, L. M. *Adv. Funct. Mater.* **2006**, *16*, 766−773.
(9) Christopher, P.; Xin, H. L.; Linic, S. *Nat. Chem.* **2011**, *3*, 467−472.
(10) Fang, Y. R.; Li, Y. Z.; Xu, H. X.; Sun, M. T. *Langmuir* **2010**, *26*, 7737−7746.
(11) Morones, J. R.; Elechiguerra, J. L.; Camacho, A.; Holt, K.; Kouri, J. B.; Ramirez, J. T.; Yacaman, M. J. *Nanotechnology* **2005**, *16*, 2346−2353.
(12) Kulkarni, A. P.; Noone, K. M.; Munechika, K.; Guyer, S. R.; Ginger, D. S. *Nano Lett.* **2010**, *10*, 1501−1505.
(13) Morfa, A. J.; Rowlen, K. L.; Reilly, T. H.; Romero, M. J.; van de Lagemaat, J. *Appl. Phys. Lett.* **2008**, *92*, 013504.
(14) Willets, K. A.; Van Duyne, R. P. *Annu. Rev. Phys. Chem.* **2007**, *58*, 267−297.
(15) Michaels, A. M.; Nirmal, M.; Brus, L. E. *J. Am. Chem. Soc.* **1999**, *121*, 9932−9939.
(16) Parfenov, A.; Gryczynski, I.; Malicka, J.; Geddes, C. D.; Lakowicz, J. R. *J. Phys. Chem. B* **2003**, *107*, 8829−8833.
(17) Homan, K. A.; Souza, M.; Truby, R.; Luke, G. P.; Green, C.; Vreeland, E.; Emelianov, S. *ACS Nano* **2012**, *6*, 641−650.
(18) Haes, A. J.; Van Duyne, R. P. *J. Am. Chem. Soc.* **2002**, *124*, 10596−10604.
(19) McFarland, A. D.; Van Duyne, R. P. *Nano Lett.* **2003**, *3*, 1057−1062.
(20) Anker, J. N.; Hall, W. P.; Lyandres, O.; Shah, N. C.; Zhao, J.; Van Duyne, R. P. *Nat. Mater.* **2008**, *7*, 442−453.
(21) Ciou, S. H.; Cao, Y. W.; Huang, H. C.; Su, D. Y.; Huang, C. L. *J. Phys. Chem. C* **2009**, *113*, 9520−9525.
(22) Zhang, Q.; Hu, Y. X.; Guo, S. R.; Goebl, J.; Yin, Y. D. *Nano Lett.* **2010**, *10*, 5037−5042.
(23) Shuford, K. L.; Ratner, M. A.; Schatz, G. C. *J. Chem. Phys.* **2005**, *123*, 114713.
(24) Jin, R. C.; Cao, Y. C.; Hao, E. C.; Metraux, G. S.; Schatz, G. C.; Mirkin, C. A. *Nature* **2003**, *425*, 487−490.
(25) Metraux, G. S.; Mirkin, C. A. *Adv. Mater.* **2005**, *17*, 412−415.
(26) Jin, R. C.; Cao, Y. W.; Mirkin, C. A.; Kelly, K. L.; Schatz, G. C.; Zheng, J. G. *Science* **2001**, *294*, 1901−1903.

(27) Wu, X. M.; Redmond, P. L.; Liu, H. T.; Chen, Y. H.; Steigerwald, M.; Brus, L. *J. Am. Chem. Soc.* **2008**, *130*, 9500−9506.
(28) Lee, G. P.; Shi, Y. C.; Lavoie, E.; Daeneke, T.; Reineck, P.; Cappel, U. B.; Huang, D. M.; Bach, U. *ACS Nano* **2013**, *7*, 5911−5921.
(29) Sun, Y. G.; Xia, Y. N. *Adv. Mater.* **2003**, *15*, 695−699.
(30) Xue, C.; Mirkin, C. A. *Angew. Chem., Int. Ed.* **2007**, *46*, 2036−2038.
(31) Xue, C.; Metraux, G. S.; Millstone, J. E.; Mirkin, C. A. *J. Am. Chem. Soc.* **2008**, *130*, 8337−8344.
(32) Aherne, D.; Ledwith, D. M.; Gara, M.; Kelly, J. M. *Adv. Funct. Mater.* **2008**, *18*, 2005−2016.
(33) Chen, S. H.; Carroll, D. L. *Nano Lett.* **2002**, *2*, 1003−1007.
(34) Chen, S. H.; Carroll, D. L. *J. Phys. Chem. B* **2004**, *108*, 5500−5506.
(35) Goebl, J.; Zhang, Q.; He, L.; Yin, Y. D. *Angew. Chem., Int. Ed.* **2012**, *51*, 552−555.
(36) Sun, Y. G.; Mayers, B.; Xia, Y. N. *Nano Lett.* **2003**, *3*, 675−679.
(37) Zhang, Q.; Yang, Y.; Li, J.; Iurilli, R.; Xie, S. F.; Qin, D. *ACS Appl. Mater. Interfaces* **2013**, *5*, 6333−6345.
(38) Washio, I.; Xiong, Y. J.; Yin, Y. D.; Xia, Y. N. *Adv. Mater.* **2006**, *18*, 1745−1749.
(39) Zhang, Q.; Li, N.; Goebl, J.; Lu, Z. D.; Yin, Y. D. *J. Am. Chem. Soc.* **2011**, *133*, 18931−18939.
(40) Cathcart, N.; Frank, A. J.; Kitaev, V. *Chem. Commun.* **2009**, 7170−7172.
(41) Tsuji, M.; Gomi, S.; Maeda, Y.; Matsunaga, M.; Hikino, S.; Uto, K.; Tsuji, T.; Kawazumi, H. *Langmuir* **2012**, *28*, 8845−8861.
(42) Li, N.; Zhang, Q.; Quinlivan, S.; Goebl, J.; Gan, Y.; Yin, Y. D. *ChemPhysChem* **2012**, *13*, 2526−2530.
(43) Wongravee, K.; Parnklang, T.; Pienpinijtham, P.; Lertvachirapaiboon, C.; Ozaki, Y.; Thammacharoen, C.; Ekgasit, S. *Phys. Chem. Chem. Phys.* **2013**, *15*, 4183−4189.
(44) Pastoriza-Santos, I.; Liz-Marzan, L. M. *Nano Lett.* **2002**, *2*, 903−905.
(45) Kilin, D. S.; Prezhdo, O. V.; Xia, Y. N. *Chem. Phys. Lett.* **2008**, *458*, 113−116.
(46) Padalkar, S.; Capadona, J. R.; Rowan, S. J.; Weder, C.; Won, Y.-H.; Stanciu, L. A.; Moon, R. J. *Langmuir* **2010**, *26*, 8497−8502.
(47) Drogat, N.; Granet, R.; Sol, V.; Memmi, A.; Saad, N.; Koerkamp, C. K.; Bressollier, P.; Krausz, P. *J. Nanopart. Res.* **2011**, *13*, 1557−1562.
(48) Ifuku, S.; Tsuji, M.; Morimoto, M.; Saimoto, H.; Yano, H. *Biomacromolecules* **2009**, *10*, 2714−2717.
(49) Diez, I.; Eronen, P.; Osterberg, M.; Linder, M. B.; Ikkala, O.; Ras, R. H. A. *Macromol. Biosci.* **2011**, *11*, 1185−1191.
(50) Martins, N. C. T.; Freire, C. S. R.; Pinto, R. J. B.; Fernandes, S. C. M.; Neto, C. P.; Silvestre, A. J. D.; Causio, J.; Baldi, G.; Sadocco, P.; Trindade, T. *Cellulose* **2012**, *19*, 1425−1436.
(51) Fortunati, E.; Armentano, I.; Zhou, Q.; Puglia, D.; Terenzi, A.; Berglund, L. A.; Kenny, J. M. *Polym. Degrad. Stab.* **2012**, *97*, 2027−2036.
(52) Lokanathan, A. R.; Uddin, K. M. A.; Rojas, O. J.; Laine, J. *Biomacromolecules* **2014**, *15*, 373−379.
(53) Dong, H.; Snyder, J. F.; Tran, D. T.; Leadore, J. L. *Carbohydr. Polym.* **2013**, *95*, 760−767.
(54) Jiang, F.; Han, S.; Hsieh, Y.-L. *RSC Adv.* **2013**, *3*, 12366−12375.
(55) Jiang, F.; Dallas, L. J.; Ahn, B. K.; Hsieh, Y.-L. *Carbohydr. Polym.* **2014**, *110*, 360−366.
(56) Hu, L. B.; Zheng, G. Y.; Yao, J.; Liu, N. A.; Weil, B.; Eskilsson, M.; Karabulut, E.; Ruan, Z. C.; Fan, S. H.; Bloking, J. T.; McGehee, M. D.; Wagberg, L.; Cui, Y. *Energy Environ. Sci.* **2013**, *6*, 513−518.
(57) Huang, J.; Zhu, H. L.; Chen, Y. C.; Preston, C.; Rohrbach, K.; Cumings, J.; Hu, L. B. *ACS Nano* **2013**, *7*, 2106−2113.
(58) Lu, P.; Hsieh, Y. L. *Carbohydr. Polym.* **2012**, *87*, 564−573.
(59) Jensen, T. R.; Duval, M. L.; Kelly, K. L.; Lazarides, A. A.; Schatz, G. C.; Van Duyne, R. P. *J. Phys. Chem. B* **1999**, *103*, 9846−9853.
(60) Sastry, M.; Mayya, K. S.; Patil, V.; Paranjape, D. V.; Hegde, S. G. *J. Phys. Chem. B* **1997**, *101*, 4954−4958.
(61) Wang, W.; Chen, X.; Efrima, S. *J. Phys. Chem. B* **1999**, *103*, 7238−7246.
(62) Yin, Y. D.; Li, Z. Y.; Zhong, Z. Y.; Gates, B.; Xia, Y. N.; Venkateswaran, S. *J. Mater. Chem.* **2002**, *12*, 522−527.
(63) Kelly, K. L.; Coronado, E.; Zhao, L. L.; Schatz, G. C. *J. Phys. Chem. B* **2003**, *107*, 668−677.
(64) Wang, M. S.; Jiang, F.; Hsieh, Y.-L.; Nitin, N. *J. Mater. Chem. B* **2014**, *2*, 6226−6235.
(65) Imai, T.; Putaux, J. L.; Sugiyama, J. *Polymer* **2003**, *44*, 1871−1879.
(66) Nishiyama, Y.; Langan, P.; Chanzy, H. *J. Am. Chem. Soc.* **2002**, *124*, 9074−9082.
(67) Fukuzumi, H.; Saito, T.; Wata, T.; Kumamoto, Y.; Isogai, A. *Biomacromolecules* **2009**, *10*, 162−165.
(68) Jiang, F.; Hsieh, Y.-L. *J. Mater. Chem. A* **2014**, *2*, 350−359.
(69) Jiang, F.; Hsieh, Y.-L. *J. Mater. Chem. A* **2014**, *2*, 6337−6342.
(70) Hildebrandt, P.; Stockburger, M. *J. Phys. Chem.* **1984**, *88*, 5935−5944.
(71) Le Ru, E. C.; Blackie, E.; Meyer, M.; Etchegoin, P. G. *J. Phys. Chem. C* **2007**, *111*, 13794−13803.